BIOCHEMISTRY
including biophysical chemistry & molecular biology

Article

pubs.acs.org/biochemistry

ABHD4 Regulates Multiple Classes of *N*-Acyl Phospholipids in the Mammalian Central Nervous System

Hyeon-Cheol Lee,*,† Gabriel M. Simon,† and Benjamin F. Cravatt*

The Skaggs Institute for Chemical Biology and Department of Chemical Physiology, The Scripps Research Institute, 10550 North Torrey Pines Road, La Jolla, California 92037, United States

Supporting Information

ABSTRACT: *N*-Acyl phospholipids are atypical components of cell membranes that bear three acyl chains and serve as potential biosynthetic precursors for lipid mediators such as endocannabinoids. Biochemical studies have implicated ABHD4 as a brain *N*-acyl phosphatidylethanolamine (NAPE) lipase, but *in vivo* evidence for this functional assignment is lacking. Here, we describe ABHD4$^{-/-}$ mice and their characterization using untargeted lipidomics to discover that ABHD4 regulates multiple classes of brain *N*-acyl phospholipids. In addition to showing reductions in brain glycerophospho-NAEs (GP-NAEs) and plasmalogen-based lyso-NAPEs (lyso-pNAPEs), ABHD4$^{-/-}$ mice exhibited decreases in a distinct set of brain lipids that were structurally characterized as *N*-acyl lysophosphatidylserines (lyso-NAPSs). Biochemical assays confirmed that NAPS lipids are direct substrates of ABHD4. These findings, taken together, designate ABHD4 as a principal regulator of *N*-acyl phospholipid metabolism in the mammalian nervous system.

Lipids serve several fundamental roles in biology, including providing the chemical matter for cell membrane structures and acting as signaling molecules that bind to protein receptors to regulate diverse physiological processes.[1] Phospholipids are a large class of lipids that contain a glycerol backbone esterified with two fatty acyl chains and conjugated through its third hydroxyl to a phosphate headgroup. The phosphate in most phospholipids is further modified with a polar substituent, such as those found in phosphatidylcholine (choline), phosphatidylethanolamine (ethanolamine), and phosphatidylserine (serine). *N*-Acyl phospholipids, however, represent an unusual class of phospholipids that contain head groups modified with fatty acids.[2,3] Two major types of *N*-acyl phospholipids have been discovered in mammals: *N*-acyl phosphatidylethanolamines (NAPEs) and *N*-acyl phosphatidylserines (NAPSs) (Figure 1). The presence of a third fatty acid group grants *N*-acyl phospholipids with substantially altered physicochemical properties compared to those of other classes of phospholipids. Although the initial structural characterization of *N*-acyl phospholipids as endogenous constituents of mammalian tissues occurred several decades ago,[4,5] we still today have only a limited understanding of the biological functions and routes for enzymatic metabolism of this class of lipids.

NAPEs are considered to be rare phospholipids and, under physiological conditions, account for ~0.01% of total phospholipids of animal membranes.[2,3] However, NAPEs can accumulate under conditions of injury or stress.[2,3] Owing to the presence of a third acyl chain, *N*-acyl phospholipids impart stabilizing properties on cell membranes[6] as well as display fusogenic potential.[7] Beyond these structural roles, some NAPEs may function as signaling molecules, as *N*-palmitoyl-

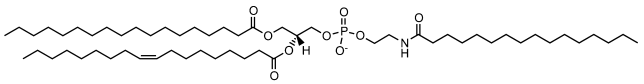

N-16:0 *sn*-1-*O*-18:0 *sn*-2-*O*-18:1 NAPE

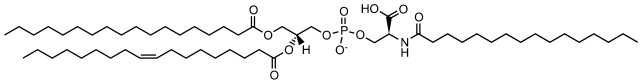

N-16:0 *sn*-1-*O*-18:0 *sn*-2-*O*-18:1 NAPS

Figure 1. *N*-Acyl phospholipids. Structures of representative *N*-acyl phosphatidylethanolamine (NAPE) and *N*-acyl phosphatidylserine (NAPS) lipids.

phosphatidylethanolamine has been shown to regulate food intake in mice[8] and inflammatory responses.[9] Arguably, however, NAPEs are most well-recognized as precursors to the *N*-acyl ethanolamine (NAE) class of signaling lipids, which includes the endocannabinoid anandamide (C20:4 NAE).[10] The conversion of NAPEs to NAEs can occur through one of multiple enzymatic routes, including direct phospholipase D-mediated catalysis by an NAPE-PLD[11−14] and multistep pathways that proceed through phospholipase $A_{1/2}$[15−17] and C[18,19] enzymes. Plasmalogen-based NAPEs (pNAPEs) are a major subclass of NAPEs and can also be catabolized by NAPE-

Received: February 27, 2015
Revised: March 20, 2015
Published: April 8, 2015

DOI: 10.1021/acs.biochem.5b00207
Biochemistry 2015, 54, 2539−2549

PLD as well as by the combined action of a pNAPE lipase and lyso-pNAPE phospholipase D.[14] The biosynthesis of NAPEs appears to involve both calcium-dependent and -independent transacylase enzymes that transfer the fatty acid groups from phospholipids onto the amine of phosphatidylethanolamine.[20−24] While the calcium-dependent transacylase remains molecularly uncharacterized, HRAS-like suppressor family proteins have been shown to function as calcium-independent transacylases that produce NAPEs.[25−32] The NAPS class of *N*-acyl phospholipids, which has been isolated from human brain, animal tissue and cells, and yeast,[33,34] is less well-characterized in terms of its biological functions and metabolism.

NAPE-PLD$^{-/-}$ mice exhibit massive increases in brain NAPE and lyso-NAPE content (∼10-fold) but only modest reductions in major NAEs (∼2-fold or less), including C16:0, C18:0, C18:1, and C20:4 NAEs.[13,14] These findings pointed to the existence of additional pathways for metabolizing NAPEs. One candidate pathway is mediated by PLA$_{1/2}$ enzymes to yield lyso-NAPE and glycerophospho (GP)-NAE intermediates, which would then be metabolized further to NAEs.[10] The serine hydrolase ABHD4 has been identified as an NAPE and lyso-NAPE lipase with strong expression in brain.[17] The function of ABHD4 *in vivo*, however, remains unknown. In this article, we describe the generation and characterization of ABHD4$^{-/-}$ mice. Lipidomic analysis of brain tissue from these animals uncovered significant reductions in not only glycerophospho-NAEs (GP-NAEs) and lyso-pNAPEs but also lyso-NAPSs. Recombinant ABHD4 was found to hydrolyze NAPS. These data thus indicate that ABHD4 is a principal enzyme responsible for the hydrolytic metabolism of both the NAPE and NAPS classes of *N*-acyl phospholipids *in vivo*.

EXPERIMENTAL PROCEDURES

Materials. Anandamide-d_4 and anandamide-d_8 were purchased from Cayman Chemicals. 1,2-Dioleoyl-*sn*-glycero-3-phosphoethanolamine (PE), 1-oleoyl-2-hydroxy-*sn*-glycero-3-phosphoethanolamine (lysoPE), 1-*O*-1′-(*Z*)-octadecenyl-2-oleoyl-*sn*-glycero-3-phosphoethanolamine (plasmenyl PE), 1-*O*-1′-(*Z*)-octadecenyl-2-hydroxy-*sn*-glycero-3-phosphoethanolamine (plasmenyl lysoPE), 1-stearoyl-2-oleoyl-*sn*-glycero-3-phosphoserine (PS), 1-stearoyl-2-hydroxy-*sn*-glycero-3-phosphoserine (lysoPS), 1-hexadecanoyl-L-serine, and 1-(5*Z*,8*Z*,11*Z*,14*Z*-eicosatetraenoyl)-L-serine were purchased from Avanti Polar Lipids (Alabaster, AL). Heptadecenoic acid, pentadecenoyl chloride, palmitoyl chloride, heptadecenoyl chloride, nonadecenoyl chloride, and arachidonoyl chloride were purchased from NuCheck Prep (Elysian, MN). 1,2-Dioleoyl-*sn*-glycero-3-phospho (*N*-nonadecenoyl) ethanolamine, 1,2-dioleoyl-*sn*-glycero-3-phospho (*N*-arachidonoyl) ethanolamine, 1-*O*-1′-(*Z*)-octadecenyl-2-oleoyl-*sn*-glycero-3-phospho (*N*-nonadecenoyl) ethanolamine, 1-oleoyl-2-hydroxy-*sn*-glycero-3-phospho (*N*-pentadecenoyl) ethanolamine, 1-oleoyl-2-hydroxy-*sn*-glycero-3-phospho (*N*-palmitoyl) ethanolamine, 1-oleoyl-2-hydroxy-*sn*-glycero-3-phospho (*N*-heptadecenoyl) ethanolamine, 1-*O*-1′-(*Z*)-octadecenyl-2-hydroxy-*sn*-glycero-3-phospho (*N*-heptadecenoyl) ethanolamine were synthesized as described.[17,35] Briefly, acid chlorides were reacted with an excess of PE, plasmenyl PE, lysoPE, or plasmenyl lysoPE and allowed to react for 1 h in CH_2Cl_2 with a catalytic amount of triethylamine. *N*-Acylated lipids were then purified by silica gel flash column chromatography or preparative TLC. 1,2-Dihydroxy-*sn*-glycero-3-phospho (*N*-pentadecenoyl) ethanolamine was synthesized by base hydrolysis of 1-oleoyl-2-hydroxy-*sn*-glycero-3-phospho (*N*-pentadecenoyl) ethanolamine as described.[17,35] The synthetic phospholipid standards were evaluated by LC-MS to assess purity and quantified by the Bartlett assay.[36] More detailed synthetic methods are described below.

Generation of ABHD4$^{-/-}$ Mice. Construction of mice bearing a disruption in the *Abhd4* gene was achieved using a standard targeting strategy in CMTI-1 embryonic stem cells from the 129S6/SvEvTac strain. Genomic DNA corresponding to a region including exons 3 and 4 of *Abhd4* was amplified from a BAC clone isolated from the RPCI-22 library. Identification of neomycin-resistant ES cell clones bearing homologous recombination events was achieved via Southern blot using a probe that hybridizes downstream of the targeting construct. Recombinant clones were injected into blastocysts from C57BL/6 mice, and germline-transmission was determined by coat color. Tail DNA from brown mice was subjected to Southern blotting using a probe that hybridizes upstream of the targeting construct, thereby confirming true homologous recombination. These mice were backcrossed into the C57BL/6 background for 10 generations prior to biochemical and lipidomic analyses.

Preparation of Mouse Tissue Proteomes. Mice were anesthetized with isoflurane and killed by decapitation. Brains were immediately removed and snap-frozen in liquid N_2. Frozen brains were dounce-homogenized on ice in PBS (pH 7.4) and centrifuged at 1000*g* for 10 min to remove debris. The resulting supernatant was further centrifuged at 100 000*g* for 45 min to provide the soluble fraction in the supernatant and the membrane fraction as a pellet. The pellet was washed and resuspended in PBS by brief sonication. Protein concentrations were determined using the DC protein assay (Bio-Rad), and samples were stored at −80 °C until use.

Gel-Based ABPP Analysis. Brain soluble and membrane proteomes (50 μg in 50 μL of PBS) were prepared from 2 week old ABHD4$^{+/+}$ and ABHD4$^{-/-}$ females and incubated with 1 μM FP-rhodamine for 30 min at 37 °C. After 30 min, reactions were quenched with 4× SDS/PAGE loading buffer (reducing), separated by SDS/PAGE [10% (w/v) acrylamide], and visualized by in-gel fluorescence scanning (Hiatchi FMBio IIe, MiraBio). Rhodamine fluorescence is shown in gray scale.

Mass Spectrometry (MS)-Based Proteomics. Serine hydrolase enrichment was performed essentially as described.[37] Briefly, brain proteomes were adjusted to a final protein concentration of 2 mg/mL and treated with FP-biotin (500 μL total reaction volume, 10 μM final concentration) for 2 h at room temperature. Excess probe was removed by protein precipitation using 4:1 (v/v) methanol/chloroform, and proteins were then dissolved in 6 M urea in 25 mM ammonium bicarbonate. Proteins were reduced with 10 mM DTT, alkylated with 40 mM iodoacetamide, and diluted to a final concentration of 2 M urea with 25 mM ammonium bicarbonate. Biotinylated proteins were then enriched with avidin beads (SIGMA; no. A9207) by incubation for 2 h at room temperature in 0.2% SDS in DPBS. The beads were washed three times with 1% SDS in DPBS and then three additional times in DPBS, and they were then resuspended in 25 mM ammonium bicarbonate with 2 M urea. On-bead digestion with 2 μg of trypsin (Promega; no. V511A) was performed overnight at 37 °C in the presence of 1 mM $CaCl_2$. Tryptic digests were acidified with 5% (v/v) formic acid, and aliquots were frozen at −80 °C until use. Multidimensional liquid chromatography tandem mass spectrometry (MudPIT)

DOI: 10.1021/acs.biochem.5b00207
Biochemistry 2015, 54, 2539−2549

analysis was performed as described previously,[38] and peptides were eluted directly into a Velos Orbitrap mass spectrometer (Thermo Fisher) essentially as previously described.[37] See Table S1 for a complete list of serine hydrolases detected in these experiments.

Cell Culture and Transfection. COS-7 cells were grown at 37 °C and 5% CO_2 to ∼70% confluence in Dulbecco's modified Eagle's medium containing 10% fetal calf serum in 10 cm dishes and transfected with 5 μg of plasmid DNA (or empty vector control) using polyethylenimine (Polysciences, Warrington, PA). After 24 h, the cells were washed twice with PBS, scraped, resuspended in PBS, and sonicated to lyse. The lysates were spun at 100 000*g* for 45 min to isolate the cytosolic fraction.

Plasmids. Full-length mouse *Abhd4* was amplified by PCR from mouse brain cDNA with primers Abhd4 forward (5′-TGGTGGAATTCGCCACCATGGGCTGGCTCAGCT-CGAC-3′) and reverse (5′-ACCTATCTAGAGTCAAC-TGAGTTGCAGATCT-3′) and was cloned into the pcDNA3.1/Myc-His vector with a C-terminal Myc-His tag using EcoRI and XbaI sites.

***In Vitro* Enzyme Assays.** Detection of (lyso)phospholipid hydrolysis was accomplished via mass spectrometric detection of the release of oleic acid or lyso-NAPE from substrates. Enzyme assays were performed in PBS in a total volume of 100 μL using 0.5 mg/mL protein. To avoid contaminating signals from endogenous lipids, soluble extracts of brain or cells were assayed. Reactions were incubated at 37 °C for 1 h with 100 μM substrate, 2 mM EDTA, with or without 0.1% Triton X-100. Reactions were stopped by the addition of 500 μL of MeOH, and 1 nmol of heptadecenoic acid or 100 pmol of 1-oleoyl-2-hydroxy-*sn*-glycero-3-phospho (*N*-heptadecenoyl) ethanolamine was added as an internal standard. Lipids were extracted by the Bligh and Dyer method.[39] A portion of the extracted lipid was injected onto an Agilent 6520 series quadrupole time-of-flight (Q-TOF) MS. Chromatography was performed on a 50 × 4.60 mm 5 μm Gemini C18 column (Phenomenex) coupled to a guard column (Gemini; C18; 4 × 3.0 mm; Phenomenex SecurityGuard cartridge). The LC method consisted of 0.1 mL/min of 100% buffer A [95:5 (v/v) H_2O/MeOH plus 0.1% (v/v) of 28% ammonium hydroxide] for 1.5 min, 0.5 mL/min linear gradient to 100% buffer B [60:35:5 (v/v/v) iPrOH/MeOH/H_2O plus 0.1% (v/v) of 28% ammonium hydroxide] over 5 min, 0.5 mL/min 100% buffer B for 5.5 min, and equilibration with 0.5 mL/min 100% buffer A for 3 min (15 min total run time). MS analysis was performed in negative scanning mode with an electrospray ionization (ESI) source. The capillary voltage was 4.0 kV, the fragmentor voltage was 100 V, the drying gas temperature was 350 °C, the drying gas flow rate was 11 L/min, and the nebulizer pressure was 45 psi. Oleic acid release or lyso-NAPE release was quantified by measuring the area under the peak and comparing it to the heptadecenoic acid or lyso-NAPE standard, respectively.

Untargeted Metabolomics Analysis. Untargeted metabolomics was performed as described previously.[40] ABHD4$^{+/+}$ and ABHD4$^{-/-}$ mice from 2 to 4 months of age (n = 4 per genotype) were anesthetized with isoflurane and killed by decapitation. Brains were harvested, laterally sectioned, and immediately submerged in liquid N_2. One frozen brain hemisphere per mouse was weighed and immediately Dounce-homogenized in 8 mL of 2:1:1 (v/v/v) $CHCl_3$/MeOH/50 mM Tris, pH 8.0, with heptadecenoic acid and anandamide-d_8 added as internal standards for negative and positive mode analysis, respectively. Homogenates were centrifuged for 10 min at 1400*g*. The organic (lower) phase was transferred to a clean vial and dried under a stream of N_2. The metabolomes were resolubilized in 2:1 v/v $CHCl_3$/MeOH (120 μL), and 30 μL was injected onto an Agilent 6520 series quadrupole time-of-flight (Q-TOF) MS. LC separation was achieved using the same solid and mobile phases described above for substrate assays. To assist in ion formation, 0.1% (v/v) of 28% ammonium hydroxide or 0.1% (v/v) formic acid was added to the buffers for negative or positive ionization mode, respectively. The LC method consisted of 0.1 mL/min 0% buffer B for 5 min, a 0.4 mL/min linear gradient over 40 min to 100% buffer B, 0.5 mL/min 100% buffer B for 10 min, and 0.4 mL/min equilibration with 0% buffer B for 5 min, for an overall run time of 60 min. MS analysis was performed with an ESI source in scanning mode from m/z = 50−1200. The capillary voltage was set to 4.0 kV, and the fragmentor voltage was set to 100 V. The drying gas temperature was 350 °C, the drying gas flow rate was 11 l/min, and the nebulizer pressure was 45 psi. Analysis of the LC-MS data were performed with the XCMS software,[41,42] which identifies, matches, aligns, and integrates chromatographic peaks and identifies m/z values that are significantly altered in control vs experimental data sets. XCMS results from two independently performed experiments were compared and filtered for m/z values that appeared in both data sets with greater than 3-fold change between genotypes, greater than 10 000 average peak-integration area, LC elution time during the linear gradient, and $P < 0.01$. Obvious isotopic peaks were manually excluded. Results are presented as the ratio of the average peak area measured in the ABHD4$^{+/+}$ vs ABHD4$^{-/-}$ brain metabolomes. Putative assignments were confirmed by coelution with synthetic standards and/or fragmentation analysis as described below. Relative abundance of known lipid species was determined by manually extracting the mass corresponding to the $[M - H]^-$ or $[M + H]^+$ parent ion (in negative or positive ionization mode, respectively), integrating the area under the peak and normalizing this value for the tissue weight and internal standard area peak. Statistical significance was determined by unpaired, two-tailed Welch's t test.

Tandem MS Fragmentation Experiments. MS/MS analysis was performed on an Agilent 6520 series quadrupole time-of-flight (Q-TOF) instrument, using the same LC separation and buffers as described above for untargeted metabolomics. MS and MS/MS data collection, both in scanning mode from m/z = 50−1200 and a rate of 1.0 spectra/s, was performed with an electrospray ionization (ESI) source. The capillary voltage was set to 4.0 kV, and the fragmentor voltage was set to 100 V. The drying gas temperature was 350 °C, the drying gas flow rate was 11 L/min, and the nebulizer pressure was 45 psi. The collision energy was set to 20 V for lyso-NAPS and 15 V for NAS.

Targeted Metabolite Measurements. NAPEs, pNAPEs, lyso-NAPEs, lyso-pNAPEs, GP-NAEs, NAEs, NAPSs, and lyso-NAPSs in brains from ABHD4$^{+/+}$ and ABHD4$^{-/-}$ mice 2 months of age were measured by multiple reaction monitoring (MRM) methods. Brains were harvested, and the metabolomes were extracted as described above. Thirty microliters of lipid extract was injected onto an Agilent 6460 series triple-quadrupole MS connected to an Agilent 1290 Infinity HPLC system. LC separation was achieved using the solid and mobile phases described above for untargeted metabolomics and the following method: 0.1 mL/min 0% buffer B for 5 min, a 0.4

DOI: 10.1021/acs.biochem.5b00207
Biochemistry 2015, 54, 2539−2549

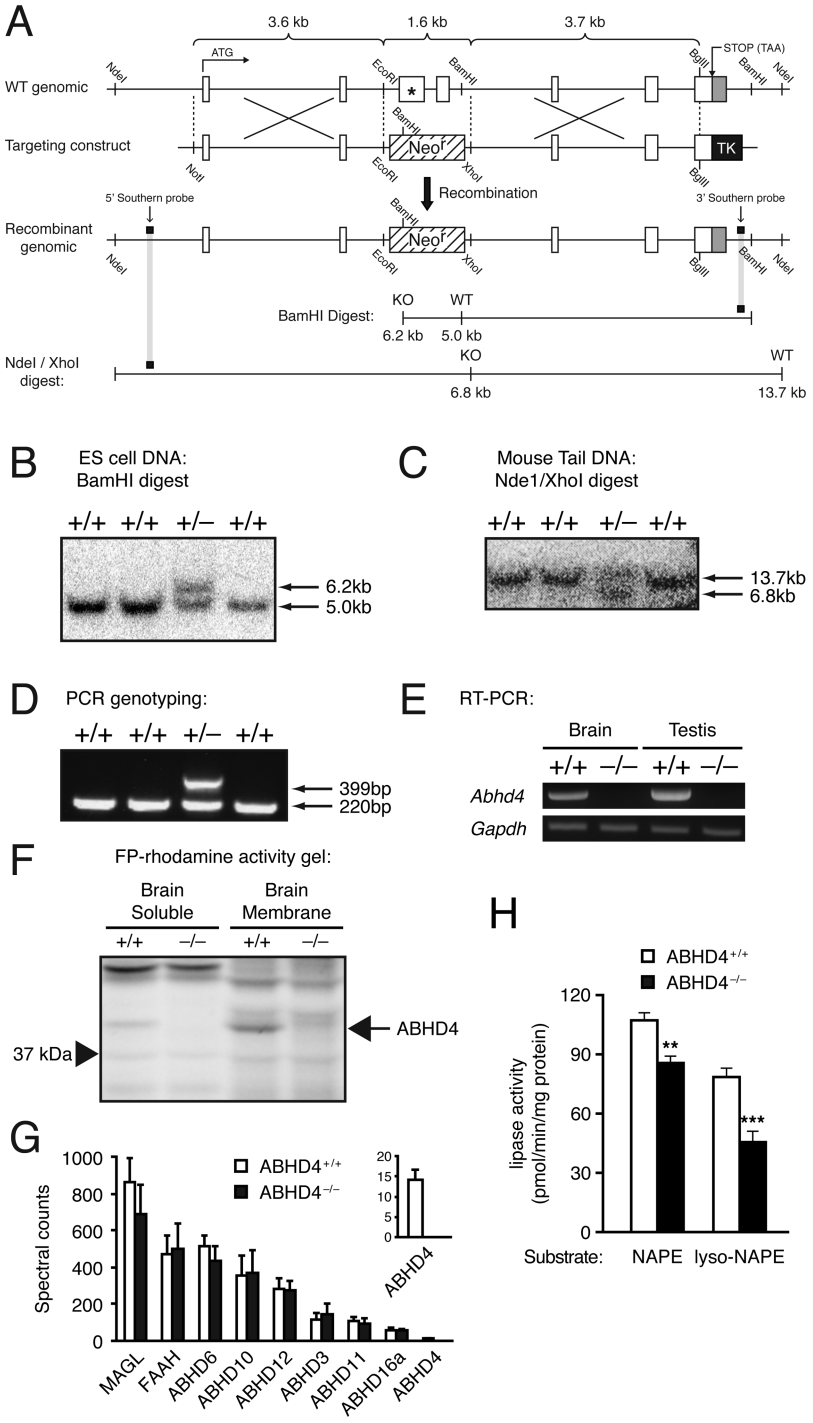

Figure 2. Generation and initial characterization of ABHD4$^{-/-}$ mice. (A) The genomic structure of the *Abhd4* genomic locus on chromosome 14 is shown, along with the targeting construct with regions of homology flanking exons 3 and 4 (which contains the catalytic serine; asterisk) and the final recombined locus. Only relevant restriction sites are designated. The positions of probes for Southern hybridization and the gene fragments expected upon Southern blotting with the indicated probes and restriction enzymes are also shown. (B) Southern blot of BamHI-digested ES cell DNA showing a clone with targeted disruption of the *Abhd4* gene. (C) Southern blot of NdeI/XhoI-digested tail DNA from ABHD4$^{+/+}$ and ABHD4$^{+/-}$ mice demonstrating germ-line transmission. (D) PCR genotyping in which the ABHD4$^{+/+}$ locus is identified by a 220 bp band and the ABHD4$^{-/-}$ locus is identified by a 399 bp band. (E) RT-PCR analysis confirmed loss of *Abhd4* mRNA expression in brain and testis tissues from ABHD4$^{-/-}$ mice. (F) ABPP of soluble and membrane fractions of brain tissue from ABHD4$^{+/+}$ and ABHD4$^{-/-}$ mice using the serine hydrolase-directed probe FP-rhodamine shows that active ABHD4 protein is not observed in ABHD4$^{-/-}$ mice. (G) Lack of ABHD4 activity in ABHD4$^{-/-}$ brains was confirmed by the MS-based proteomic method ABPP-MudPIT using the probe FP-biotin. The activity of representative serine hydrolases is shown. See Table S1 for a complete list of detected serine hydrolases. (H) Soluble fractions of brain tissue from ABHD4$^{+/+}$ and ABHD4$^{-/-}$ mice were incubated with NAPE (1,2-dioleoyl-*sn*-glycero-3-phospho (*N*-arachidonoyl) ethanolamine) or lyso-NAPE (1-oleoyl-2-hydroxy-*sn*-glycero-3-phospho (*N*-palmitoyl) ethanolamine), and hydrolytic activity was quantified by measuring lyso-NAPE and oleic acid release, respectively. Data represent mean values ± SEM (n = 5). **, P < 0.01; ***, P < 0.001. Unpaired, two-tailed t-test was used.

DOI: 10.1021/acs.biochem.5b00207
Biochemistry 2015, 54, 2539–2549

mL/min linear gradient over 15 min to 100% buffer B, 0.5 mL/min 100% buffer B for 8 min, and 0.4 mL/min equilibration with 0% buffer B for 5 min (33 min total run time per sample). For measurements in negative mode, 0.1% (v/v) of 28% ammonium hydroxide was added to the buffers. For measurements in positive mode, 0.1% (v/v) of formic acid or 10 mM ammonium formate was added to the buffers. For NAPEs and pNAPEs, MRM transition from $[M - H]^-$ to the fragment ion $[R_2COO]^-$ with collision energy 45 V was used. Absolute abundance of NAPEs and pNAPEs were estimated by comparison to the *N*-19:1 NAPE (1,2-dioleoyl-*sn*-glycero-3-phospho (*N*-nonadecenoyl) ethanolamine) standard. For pNAPEs, the extraction and ionization efficiencies of *N*-19:1 pNAPE (1-*O*-1′-(*Z*)-octadecenyl-2-oleoyl-*sn*-glycero-3-phospho (*N*-nonadecenoyl) ethanolamine) were compared to those of the *N*-19:1 NAPE standard, and the levels of pNAPEs were corrected accordingly. For lyso-NAPEs, MRM transition from $[M - H]^-$ to the fragment ion $[R_1COO]^-$ or $[R_2COO]^-$ with collision energy 35 V was used. Absolute abundance of lyso-NAPEs was estimated by comparison to the *N*-17:1 lyso-NAPE (1-oleoyl-2-hydroxy-*sn*-glycero-3-phospho (*N*-heptadecenoyl) ethanolamine) standard. For GP-NAEs, MRM transition from $[M - H]^-$ to the fragment ion [deprotonated glycerophosphate]$^-$ at *m*/*z* 171 with collision energy 24 V was used. Absolute abundance of GP-NAEs was estimated by comparison to the *N*-15:1 GP-NAE (1,2-dihydroxy-*sn*-glycero-3-phospho (*N*-pentadecenoyl) ethanolamine) standard. Extraction efficiencies for *N*-15:1, *N*-16:0, *N*-18:0, and *N*-18:1 GP-NAEs under these conditions were 2.3, 10.5, 36.6, and 22.0%, respectively, and endogenous GP-NAE levels were corrected accordingly. For certain GP-NAE measurements (Figure S1B), 1% formic acid was used for the aqueous phase of the lipid extraction, rather than Tris, pH 8. Under these conditions, extraction efficiencies for *N*-15:1, *N*-16:0, *N*-18:0, and *N*-18:1 GP-NAEs were 62.2, 78.2, 83.4, and 78.9%, respectively, and measurements of endogenous species were corrected accordingly. For NAPSs, MRM transition from $[M - H]^-$ to the fragment ion [phosphatidic acid]$^-$ (loss of *N*-acyl serine) with collision energy 35 V was used. Absolute abundance of NAPSs was estimated by comparison to the *N*-17:1 NAPS (1-stearoyl-2-oleoyl-*sn*-glycero-3-phospho (*N*-heptadecenoyl) serine) standard. For lyso-NAPSs, MRM transition from $[M - H]^-$ to the fragment ion [lyso phosphatidic acid]$^-$ (loss of *N*-acyl serine) with collision energy 20 V was used. Abundance of lyso-NAPSs was compared to the internal *N*-17:1 lyso-NAPS (1-stearoyl-2-hydroxy-*sn*-glycero-3-phospho (*N*-heptadecenoyl) serine) standard; however, the amount of synthesized *N*-17:1 lyso-NAPS standard was too low to permit absolute quantitation, so the values are reported as arbitrary units. For NASs, MRM transition from $[M - H]^-$ to the fragment ion $[C_2H_4NO_2]^-$ with collision energy 15 V was used. Absolute abundance of NASs was estimated by comparison to the *N*-17:1 NAS (1-heptadecenoyl-L-serine) standard. For NAEs, formic acid was included in the mobile phase and MRM transition from $[M + H]^+$ to *m*/*z* 62 (ethanolamine fragment) with collision energy 11 V was used, except for the anandamide-d_4 standard, which monitored the transition from $[M + H]^+$ to *m*/*z* 66 (ethanolamine-d_4 fragment). NAEs were quantified by comparison to the anandamide-d_4 standard. For lyso-pNAPEs, ammonium formate was added to the buffers and MRM transition from $[M + H]^+$ to $[CH_2CH_2NHCOR_N]^+$ with collision energy 15 V was used. Absolute abundance of lyso-pNAPEs was estimated by comparison to the *N*-17:1 lyso-NAPE standard. The extraction and ionization efficiencies of *N*-17:1 lyso-pNAPE (1-*O*-1′-(*Z*)-octadecenyl-2-hydroxy-*sn*-glycero-3-phospho (*N*-heptadecenoyl) ethanolamine) were compared to those of the *N*-17:1 lyso-NAPE standard, and the levels of lyso-pNAPEs were corrected accordingly. MS analyses were performed by multiple reaction monitoring (MRM) with an ESI source. The capillary voltage was set to 3.5 kV, and the fragmentor voltage was set to 100 V. The drying gas temperature was 350 °C, the drying gas flow rate was 9 L/min, and the nebulizer pressure was 45 psi. The dwell time for each lipid was set to 100 ms.

Chemical Syntheses of Lipid Standards and Substrates. *Synthesis of 1-Stearoyl-2-hydroxy-sn-glycero-3-phospho(N-palmitoyl) Serine.* A solution of 1-stearoyl-2-hydroxy-*sn*-glycero-3-phosphoserine (3.0 mg, 5.7 μmol, 1.0 equiv) in CH_2Cl_2 (1 mL) and triethylamine (12.5 μL) was treated with palmitoyl chloride (1.4 mg, 5.1 μmol, 0.9 equiv), and the reaction mixture was stirred for 1 h at ambient temperature. The reaction was concentrated under a stream of N_2, and the remaining residue was purified by preparative TLC ($CHCl_3$/MeOH/NH_4OH/H_2O = 65:35:5:1), providing the title compound. HRMS (ESI-TOF$^-$) *m*/*z* calcd for $C_{40}H_{77}NO_{10}P$ $[M - H]^-$, 762.5290; found, 762.5297. 1-Stearoyl-2-oleoyl-*sn*-glycero-3-phospho (*N*-palmitoyl) serine HRMS (ESI-TOF$^-$) *m*/*z* calcd for $C_{58}H_{109}NO_{11}P$ $[M - H]^-$, 1026.7743; found, 1026.7746. 1-Stearoyl-2-oleoyl-*sn*-glycero-3-phospho (*N*-heptadecenoyl) serine HRMS (ESI-TOF$^-$) *m*/*z* calcd for $C_{59}H_{109}NO_{11}P$ $[M - H]^-$, 1038.7743; found, 1038.7743. 1-Stearoyl-2-hydroxy-*sn*-glycero-3-phospho (*N*-heptadecenoyl) serine HRMS (ESI-TOF$^-$) *m*/*z* calcd for $C_{41}H_{77}NO_{10}P$ $[M - H]^-$, 774.5290; found, 774.5286. Each was synthesized from its corresponding PS and lyso-PS analogues and characterized in the same manner.

Synthesis of 1-Heptadecenoyl-L-serine (N-17:1 NAS). L-Serine (27.4 mg, 0.26 mmol, 1.5 equiv) was dissolved in 2 M NaOH (0.4 mL, 4.6 equiv), and THF (0.4 mL) was added. The mixture was stirred on ice for 10 min, and heptadecenoyl chloride dissolved in 0.2 mL of THF (49.9 mg, 0.174 mmol, 1.0 equiv) was added dropwise. The mixture was stirred for 1 h at ambient temperature and then poured into ice-cold HCl. The product was extracted with EtOAc, and the combined organic layers were dried over anhydrous Na_2SO_4 and concentrated under reduced pressure. The residue was purified by preparative TLC ($CHCl_3$/MeOH/NH_4OH/H_2O = 65:35:5:1), providing the title compound as a white solid (25.0 mg, 40%): ^{1}H NMR (600 MHz, $CDCl_3$) δ 5.36 (s, 2H), 4.34 (s, 1H), 3.99 (s, 1H), 3.76 (s, 1H), 1.21−2.37 (m, 26H), 0.91 (m, 3H). HRMS (ESI-TOF$^-$) *m*/*z* calcd for $C_{20}H_{36}NO_4$ $[M - H]^-$, 354.2649; found, 354.2648.

RESULTS AND DISCUSSION

Generation and Initial Characterization of ABHD4$^{-/-}$ Mice. ABHD4$^{-/-}$ mice were generated by replacing exons three and four of the *Abhd4* gene (exon three encodes the catalytic serine) with a Neo cassette using traditional gene-targeting techniques (Figure 2A). Disruption of the genomic locus was confirmed by Southern blotting (Figure 2B,C) and PCR genotyping (Figure 2D). Loss of *Abhd4* mRNA expression and ABHD4 protein activity were confirmed by RT-PCR (Figure 2E) and activity-based protein profiling [ABPP; gel-based (Figure 2F) and mass spectrometry (MS)-based (Figure 2G and Table S1)]. ABHD4$^{-/-}$ mice were born at the expected Mendelian frequency, were viable and healthy,

DOI: 10.1021/acs.biochem.5b00207
Biochemistry 2015, 54, 2539−2549

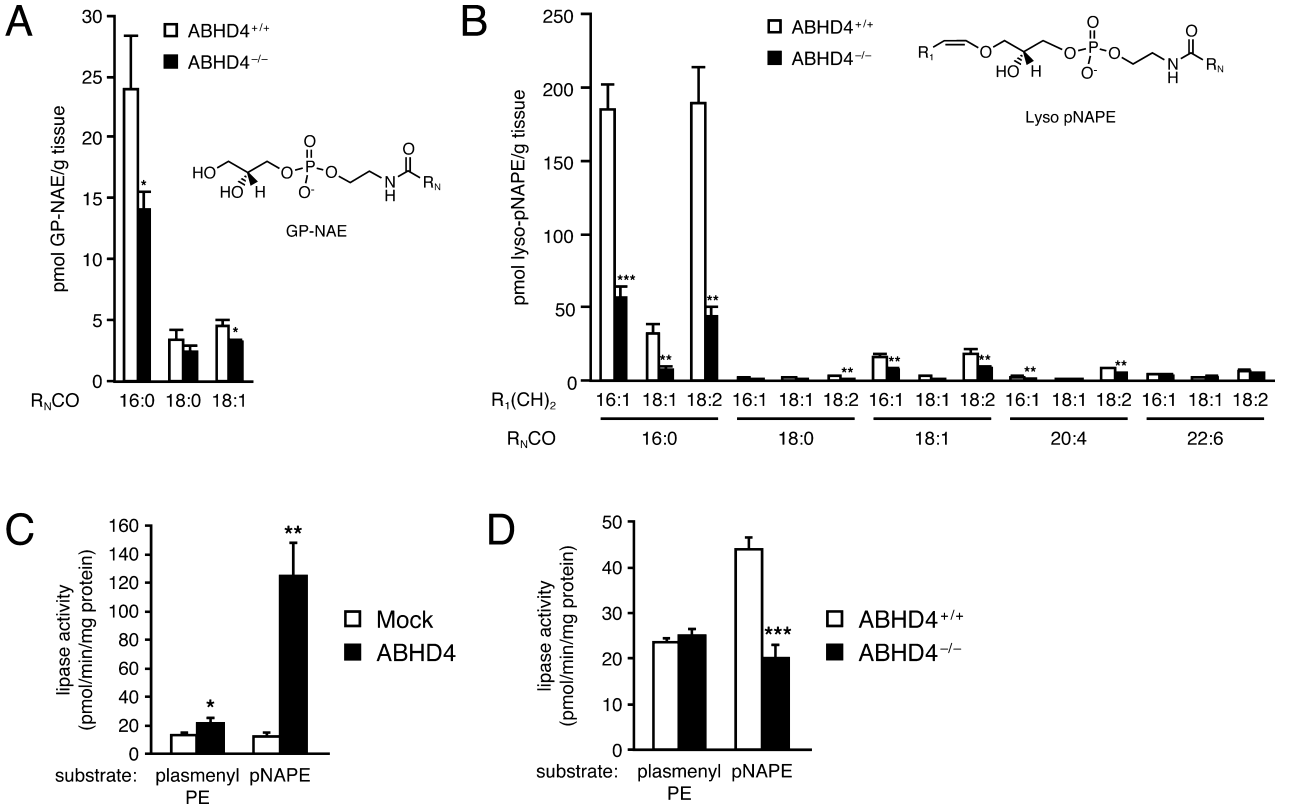

Figure 3. GP-NAEs and lyso-pNAPEs are decreased in brain tissue from ABHD4$^{-/-}$ mice. (A, B) Targeted mass-spectrometry-based estimates of GP-NAE (A) and lyso-pNAPE (B) abundance in brain tissue from ABHD4$^{+/+}$ and ABHD4$^{-/-}$ mice. Data represent mean values ± SEM (n = 8 for A; n = 5 for B). *, P < 0.05; **, P < 0.01; ***, P < 0.001. Unpaired, two-tailed t-test was used. (C, D) Soluble fractions of mock- and ABHD4-transfected COS-7 cell extracts (C) or brain tissue from ABHD4$^{+/+}$ and ABHD4$^{-/-}$ mice (D) were incubated with plasmenyl PE (1-O-1′-(Z)-octadecenyl-2-oleoyl-sn-glycero-3-phosphoethanolamine) or pNAPE (1-O-1′-(Z)-octadecenyl-2-oleoyl-sn-glycero-3-phospho (N-palmitoyl) ethanolamine), and hydrolytic activity was quantified by measuring oleic acid release. Data represent mean values ± SEM (n = 4). *, P < 0.05; **, P < 0.01; ***, P < 0.001. Unpaired, two-tailed t-test was used. See also Figure S1.

and showed no overt differences in their cage behavior compared to that of wild-type littermates. Brain homogenates from ABHD4$^{-/-}$ mice displayed significant, but incomplete, reductions in NAPE- and lyso-NAPE-lipase activity compared to that in brain homogenates from ABHD4$^{+/+}$ mice (Figure 2H), indicating that ABHD4 is a principal, but not sole, enzyme in the nervous system that hydrolyzes NAPEs and lyso-NAPEs.

Deregulated Brain NAPE Metabolism in ABHD4$^{-/-}$ Mice. We previously showed that ABHD4 exhibits both NAPE- and lyso-NAPE-lipase activity *in vitro* to sequentially produce lyso-NAPEs and GP-NAEs,[17] the latter of which can be processed further to NAEs by glycerophosphodiesterase such as GDE1.[35,43] On the basis of these biochemical assignments, we measured the major classes of lipids along the NAPE metabolic pathway in brain tissue from ABHD4$^{+/+}$ and ABHD4$^{-/-}$ mice. No changes in NAPE or NAE content were observed in ABHD4$^{-/-}$ brains (Figure S1). In contrast, the concentrations of multiple GP-NAEs were significantly reduced in ABHD4$^{-/-}$ brains compared to that in wild-type brains, with the decrease in N-16:0 GP-NAE being the most prominent (Figures 3A and S1). The absolute concentrations of GP-NAEs were affected by the pH of the aqueous phase of the lipid extraction (see below), but, regardless, significant reductions were observed with or without acidification of the aqueous phase (Figures 3A and S1). Modest, but significant, reductions in some lyso-NAPEs, including N-16:0, O-18:0 and N-16:0, O-20:4, were also detected in brains from ABHD4$^{-/-}$ mice (Figure S1).

There are two primary classes of ethanolamine glycerophospholipids: diacyl-PEs and 1-alkenyl 2-acyl PEs (plasmalogens). Plasmalogen-type NAPE and lyso-NAPE (pNAPE and lyso-pNAPE, respectively) are also present in mouse brain, and NAEs can be formed from these lipids through both NAPE-PLD-dependent and -independent pathways.[14] In contrast to the aforementioned minor reductions in lyso-NAPEs, the lyso-pNAPE content of ABHD4$^{-/-}$ brains was markedly decreased (Figure 3B). We found that recombinant ABHD4 expressed by transient transfection in COS-7 cells showed robust pNAPE-lipase activity (Figure 3C) and that brain lysates from ABHD4$^{-/-}$ mice exhibited significantly decreased pNAPE-lipase activity (Figure 3D). Recombinant ABHD4 displayed, on the other hand, a very limited capacity to hydrolyze plasmenyl-PE (Figure 3C), and the hydrolytic activity for this substrate was unaltered in ABHD4$^{-/-}$ brain tissue (Figure 3D). Despite substantial reductions in lyso-pNAPEs, the concentrations of pNAPEs were unaltered in brain tissue from ABHD4$^{-/-}$ mice (Figure S1).

As mentioned above, acidification of the aqueous phase during lipid extraction resulted in higher absolute concentrations of GP-NAEs and a more prominent decrease in these concentrations in ABHD4$^{-/-}$ brains that resembled the magnitude of reductions observed in brain lyso-pNAPEs. On the basis of the known vulnerability of plasmalogen alkenyl

DOI: 10.1021/acs.biochem.5b00207
Biochemistry 2015, 54, 2539−2549

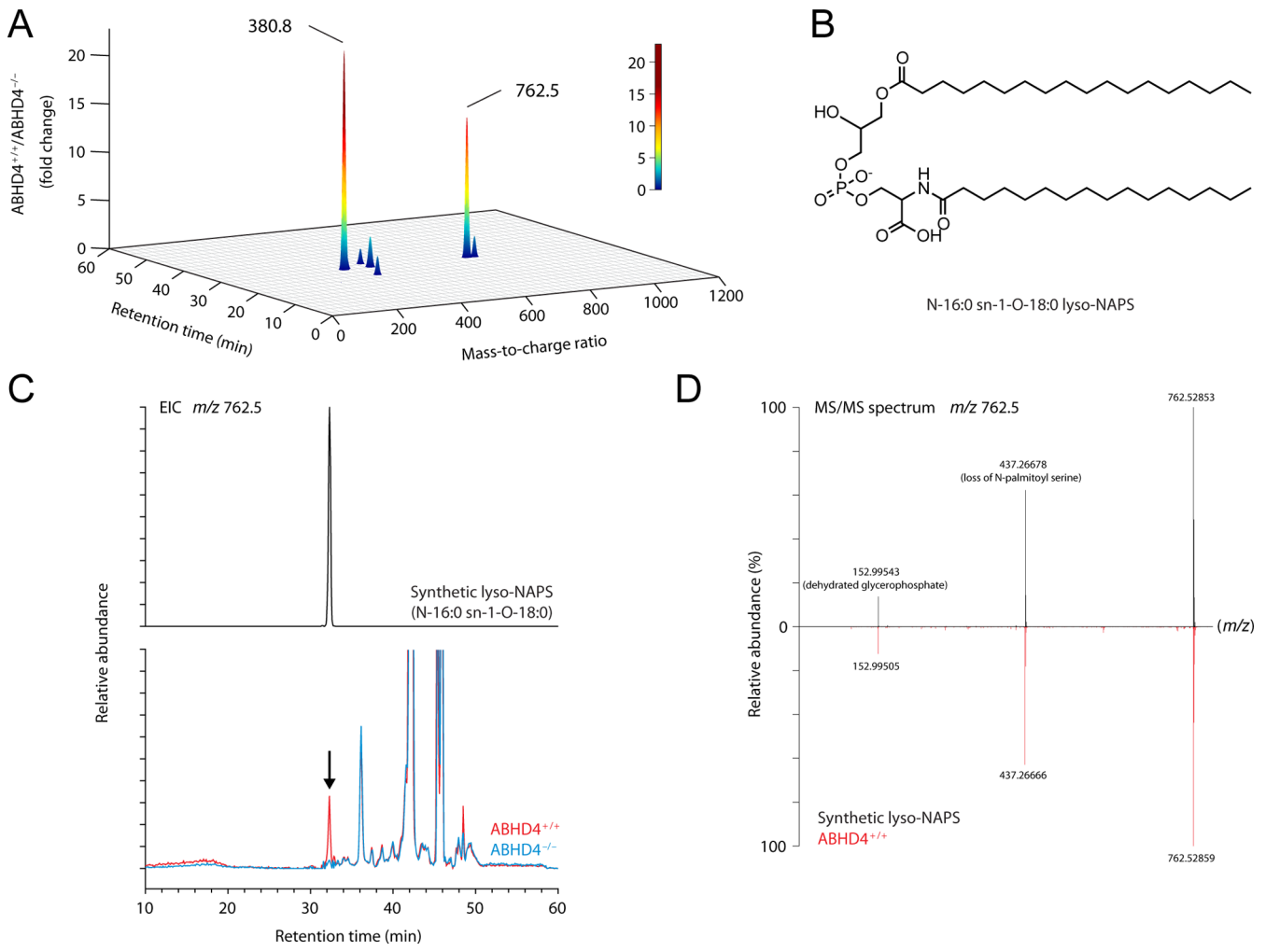

Figure 4. Lipidomic analysis of ABHD4$^{-/-}$ mice brains. (A) Changes in brain metabolites in ABHD4$^{+/+}$ versus ABHD4$^{-/-}$ brains were measured by untargeted LC-MS. A metabolite with *m/z* 380.8 and 762.5 was profoundly decreased in brains from ABHD4$^{-/-}$ mice compared with that in ABHD4$^{+/+}$ mice. (B) Structure of *N*-16:0/*sn*-1-*O*-18:0 lyso-NAPS (1-stearoyl-2-hydroxy-*sn*-glycero-3-phospho (*N*-palmitoyl) serine). (C, D) The *m/z* 762.5 metabolite (red trace) in brain tissue from ABHD4$^{+/+}$ mice exhibited the same LC elution time (C) and MS/MS fragmentation pattern (D) as that of a synthetic *N*-16:0 *O*-18:0 lyso-NAPS standard (black trace). The decrease of the *m/z* 762.5 metabolite in ABHD4$^{-/-}$ mice is also shown (blue trace). Key daughter ions in the MS/MS analysis include 153.0 (dehydrated glycerophosphate) and 437.3 [loss of *N*-palmitoyl serine (*O*-18:0 lysophosphatidic acid)].

bonds to acid cleavage,[44] we speculate that acid-catalyzed breakdown of the *sn*-1 alkenyl bond of lyso-pNAPEs may contribute to accumulated GP-NAE signals under acid extraction conditions.

These data, taken together, demonstrate that ABHD4 regulates multiple, but not all, components of the NAPE pathway. The substantial reductions in GP-NAEs and lyso-pNAPEs in ABHD4$^{-/-}$ brains support a physiological role for ABHD4 as a principal (lyso)-NAPE lipase in the mammalian nervous system. The more modest reductions in lyso-NAPEs could be explained by a dual role for ABHD4 in contributing to both the biosynthesis and degradation of this class of lipids (through NAPE and lyso-NAPE hydrolysis, respectively), which is not a complication for lyso-pNAPEs, since these ether lipids cannot be further hydrolyzed by ABHD4. That neither brain NAPE nor pNAPE were substantially affected by ABHD4 disruption (Figure S1D, E) could reflect the involvement of other metabolic pathways that control the steady-state concentrations of these lipids, such as their direct conversion to NAEs by NAPE-PLD,[13,14] or a consequence of the much larger concentrations of (p)NAPEs compared to that of their downstream lyso-(p)NAPE and GP-NAE products.

Lipidomics Identifies Deregulated NAPS Metabolism in ABHD4$^{-/-}$ Brains. We more fully characterized the metabolic changes that occur in brains from ABHD4$^{-/-}$ mice by performing untargeted MS-based lipidomic experiments. Briefly, lipid extracts were prepared using a modified Folch extraction[45] in which frozen tissue was homogenized in 2:1:1 chloroform/methanol/buffer and the lipid-containing organic layer was evaporated to dryness. Lipid extracts were analyzed by LC-MS using reverse-phase chromatography and high-resolution MS in both positive and negative modes across a mass range from 50 to 1200 *m/z* units. XCMS software[42] was employed to align chromatograms across multiple independent LC-MS runs and identify substantial (>3-fold) and statistically significant ($P < 0.01$) differences in *m/z* value peaks between the ABHD4$^{+/+}$ and ABHD4$^{-/-}$ brain tissues. Using this approach, a major difference was observed in the negative ion mode with mass-to-charge (*m/z*) ratios of 380.8 and 762.5 (likely representing the $[M - 2H]^{2-}$ and $[M - H]^{-}$ ions of the

DOI: 10.1021/acs.biochem.5b00207
Biochemistry 2015, 54, 2539−2549

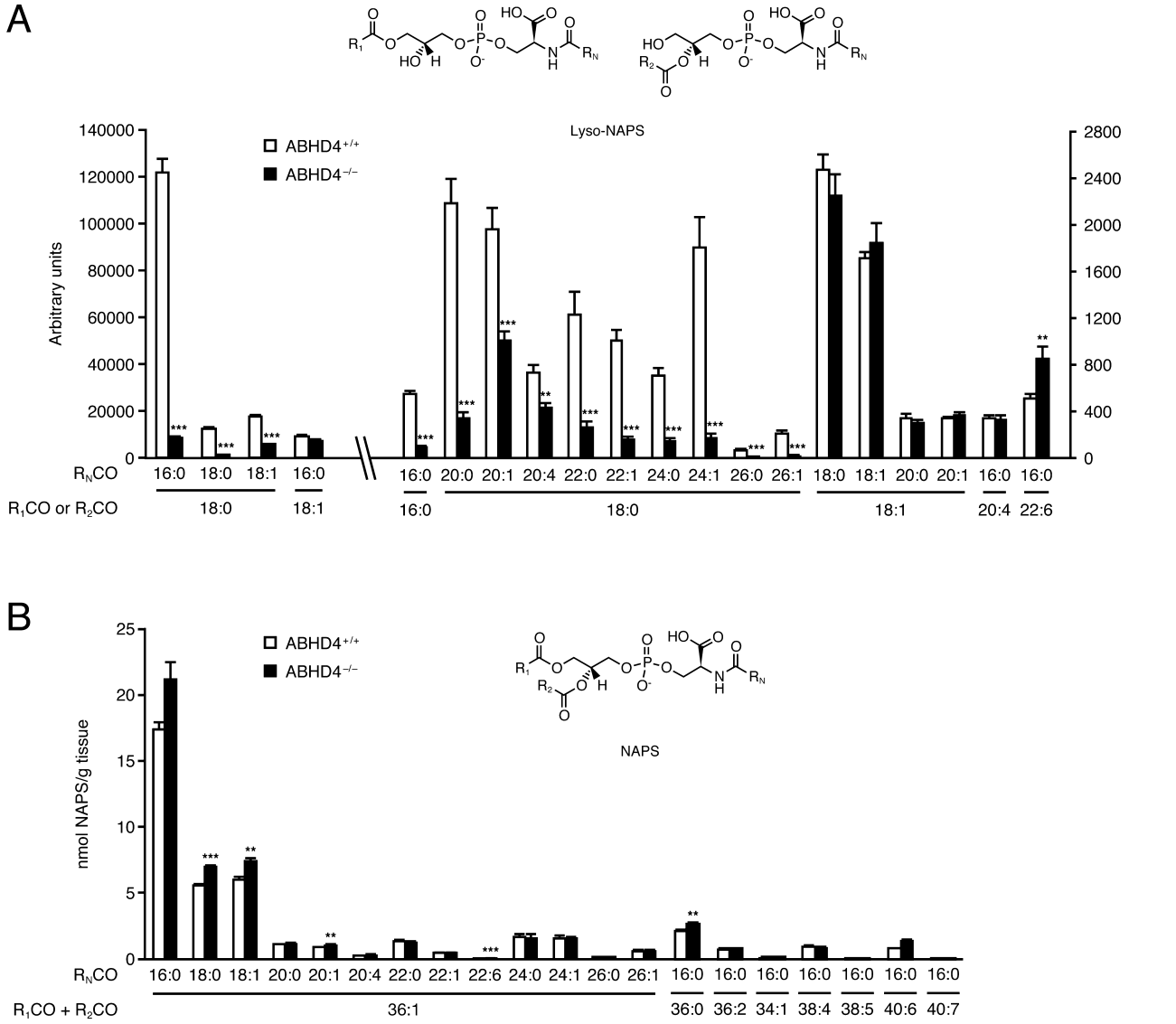

Figure 5. Lyso-NAPSs are decreased in brain tissue from ABHD4$^{-/-}$ mice. Targeted MS-based estimates of lyso-NAPS (A) and NAPS (B) abundance in brain tissue from ABHD4$^{+/+}$ and ABHD4$^{-/-}$ mice. Lyso-NAPS measurements are reported in arbitrary units. Data represent mean values ± SEM (n = 8 for A; n = 5 for B). **, P < 0.01; ***, P < 0.001. Unpaired, two-tailed t-test was used.

same metabolite) (Figure 4A). This metabolite was substantially reduced in brains from ABHD4$^{-/-}$ mice (Figure 4A and Table S2). Several candidate structures for this metabolite were considered, including phospholipids (PE and PS), lyso-NAPEs, and lyso-NAPSs, among others. Chemical synthesis of *N*-16:0/*O*-22:6 lyso-NAPE and *N*-16:0/*O*-18:0 lyso-NAPS (Figure 4B), which have the same nominal mass of 762, provided material for comparison with the endogenous m/z 762.5 metabolite. These analyses revealed that the endogenous m/z 762.5 metabolite coeluted with *N*-16:0/*O*-18:0 lyso-NAPS (Figure 4C), whereas the retention times of the isobaric PE, lyso-NAPE, and PS species were clearly distinct (data not shown). The endogenous m/z 762.5 metabolite also gave an identical tandem MS fragmentation pattern compared to that of synthetic *N*-16:0/*O*-18:0 lyso-NAPS (Figure 4D).

Taken together, these lipidomic and follow-up analytical studies indicate that ABHD4 regulates *N*-16:0/*O*-18:0 lyso-NAPS content in mouse brain.

Deregulated Brain NAPS Metabolism in ABHD4$^{-/-}$ Mice. We next performed a broader analysis of lyso-NAPS species in ABHD4$^{+/+}$ and ABHD4$^{-/-}$ brain tissues by targeted (multiple reaction monitoring) MS. Nearly all of the *O*-16:0 and *O*-18:0 lyso-NAPS species were dramatically reduced in brain tissue from ABHD4$^{-/-}$ mice, including the most abundant detected species *N*-16:0, *O*-18:0 (Figure 5A). In contrast, lyso-NAPS species with unsaturated *O*-fatty acyl groups on the glycerol backbone were unchanged in ABHD4$^{-/-}$ brain tissue. Conversely, modest, but significant, elevations were observed in several NAPS lipids in ABHD4$^{-/-}$ brain tissue (Figure 5B). Considering that unsaturated fatty acids are generally attached at *sn*-2 position of phospholipids, these lipid profiles suggest that ABHD4 hydrolyzes the *sn*-2 fatty acyl chain of *N*-acyl phosphatidylserines (NAPSs) to produce *sn*-1-*O*-saturated lyso-NAPSs.

NAPSs are potential precursors of *N*-acyl serines (NASs), a class of bioactive lipids implicated in inflammation,[46] neuroprotection,[47,48] and bone maintenance.[49] We did not, however, observe differences in NAS content between ABHD4$^{+/+}$ and ABHD4$^{-/-}$ brain tissues (Figure S2).

DOI: 10.1021/acs.biochem.5b00207
Biochemistry 2015, 54, 2539−2549

NAPS Is a Direct Substrate of ABHD4. To determine whether ABHD4 acted as an NAPS lipase, we next measured the NAPS hydrolytic activity of lysates from mock- and ABHD4-transfected COS-7 cells and found that the latter samples showed significantly elevated NAPS lipase activity when assayed either in the presence or absence of Triton X-100 as a detergent (Figures 6A and S3). Inclusion of Triton X-100 as a detergent proportionally increased the NAPS hydrolytic activities of both mock- and ABHD4-transfected lysates (Figures 6A and S3). No differences were detected in the PS lipase activity of mock- and ABHD4-transfected COS-7 cell lysates in the presence or absence of Triton X-100 (Figure 6A). The NAPS lipase activity of brain tissue was also substantially increased in the presence of Triton X-100, and, under these conditions, a significant reduction in NAPS (Figures 6B and S3) and (lyso)-NAPE hydrolysis (Figure S3) was detected in ABHD4$^{-/-}$ brain lysates. These data, taken together, indicate that ABHD4 serves as a general *N*-acyl phospholipid hydrolase capable of accepting both NAPEs and NAPSs as substrates. That brain tissue from ABHD4$^{-/-}$ mice still exhibits considerable *N*-acyl phospholipase activity (Figures 2H, 3D, S3, and 6B), however, points to the existence of additional lipases that may contribute to NAPE and NAPS metabolism *in vivo*.

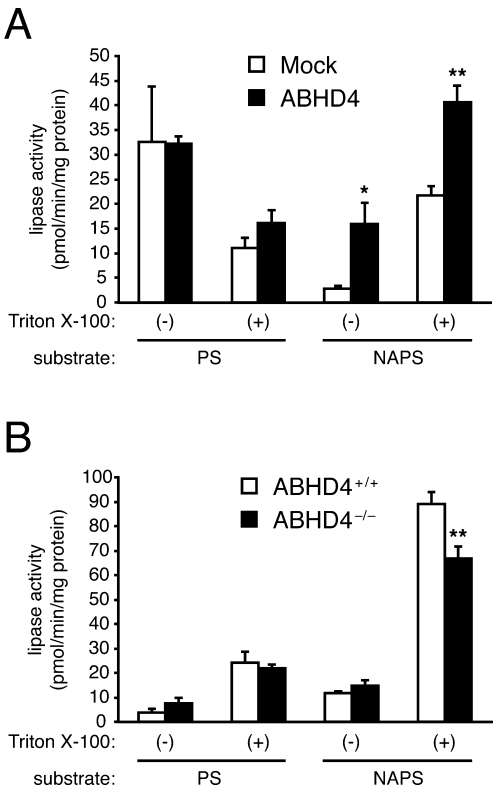

Figure 6. ABHD4 exhibits NAPS-lipase activity. Soluble fractions of mock- and ABHD4-transfected COS-7 cell extracts (A) or brain tissue from ABHD4$^{+/+}$ and ABHD4$^{-/-}$ mice (B) were incubated with PS (1-stearoyl-2-oleoyl-*sn*-glycero-3-phosphoserine) or NAPS (1-stearoyl-2-oleoyl-*sn*-glycero-3-phospho (*N*-palmitoyl) serine), and hydrolytic activity was quantified by measuring oleic acid release in the absence or presence of 0.1% of Triton X-100. See, also, Figure S3 for measurement of NAPS hydrolysis by quantifying release of lyso-NAPS product. Data represent mean values ± SEM (n = 4 for A; n = 5 for B). *, $P < 0.05$; **, $P < 0.01$. Unpaired, two-tailed t-test was used.

CONCLUSIONS

Our studies provide strong evidence that ABHD4 is a principal enzyme responsible for *N*-acyl phospholipid metabolism in the nervous system. The contribution of ABHD4 appears to be complementary to that of NAPE-PLD in that disruption of ABHD4 primarily affects lyso-(p)NAPE and lyso-NAPS content, whereas disruption of NAPE-PLD causes dramatic elevations in (p)NAPEs and lyso-(p)NAPEs.[13,14] Ablation of either enzyme alone is insufficient to produce large changes in major NAEs (e.g., C16:0, C18:0, C18:1) or anandamide, possibly indicating that these pathways can compensate for another or that additional enzymes also participate in the biosynthesis of NAEs. Future studies with NAPE-PLD$^{-/-}$/ABHD4$^{-/-}$ mice should help to address this question.

Several studies have implicated the direct involvement of NAPEs in cellular and physiological processes,[2,3] including feeding,[8] inflammation,[9] and biomembrane stability.[6] Lyso-(p)NAPEs are less well-characterized. NAPSs were only recently identified as natural brain constituents,[33,50] and, to our knowledge, lyso-NAPSs have not previously been reported as endogenous metabolites in mammalian systems. Knockdown of ABHD4 has been shown to confer resistance to anoikis (or cell-detachment-induced apoptosis) in RWPE-1 prostate cells.[51] Whether this effect is mediated by *N*-acyl phospholipids, however, remains unknown. Future studies using ABHD4$^{-/-}$ mice, as well as the development of ABHD4-selective inhibitors, should strengthen our understanding of the functions of this enzyme and its *N*-acyl phospholipid substrates and products in mammalian biology and disease.

ASSOCIATED CONTENT

Supporting Information

Table S1: ABPP-MudPIT analysis of serine hydrolase activities in brains from ABHD4$^{+/+}$ and ABHD4$^{-/-}$ mice. Table S2: Untargeted lipidomic profiling of ABHD4$^{+/+}$ and ABHD4$^{-/-}$ brain tissue. Figure S1: NAE, lyso-NAPE, GP-NAE, NAPE, and pNAPE content of brain tissue from ABHD4$^{+/+}$ and ABHD4$^{-/-}$ mice. Figure S2: NAS content of brain tissue from ABHD4$^{+/+}$ and ABHD4$^{-/-}$ mice. Figure S3: (Lyso) *N*-acyl phospholipid lipase activities of ABHD4-transfected cells and brain tissue from ABHD4$^{+/+}$ and ABHD4$^{-/-}$ mice. This material is available free of charge via the Internet at http://pubs.acs.org.

AUTHOR INFORMATION

Corresponding Authors

*(H.-C.L.) E-mail: hclee@scripps.edu.
*(B.F.C.) E-mail: cravatt@scripps.edu.

Author Contributions

†H.-C.L. and G.M.S. contributed equally to this work.

Funding

This work was supported by the National Institutes of Health, grant R01 DA033760 (B.F.C.), and a Japanese Society for the Promotion of Science Scholarship (H.-C.L.).

Notes

The authors declare no competing financial interest.

ACKNOWLEDGMENTS

We thank K.-L. Hsu for helpful discussions and K. Masuda, H. Pugh, T. Kambe, K. Lum, and D. Ogasawara for technical assistance.

DOI: 10.1021/acs.biochem.5b00207
Biochemistry 2015, 54, 2539−2549

REFERENCES

(1) Muro, E., Atilla-Gokcumen, G. E., and Eggert, U. S. (2014) Lipids in cell biology: how can we understand them better? *Mol. Biol. Cell 25*, 1819−1823.

(2) Wellner, N., Diep, T. A., Janfelt, C., and Hansen, H. S. (2013) N-Acylation of phosphatidylethanolamine and its biological functions in mammals. *Biochim. Biophys. Acta 1831*, 652−662.

(3) Coulon, D., Faure, L., Salmon, M., Wattelet, V., and Bessoule, J. J. (2012) Occurrence, biosynthesis and functions of N-acylphosphatidylethanolamines (NAPE): not just precursors of N-acylethanolamines (NAE). *Biochimie 94*, 75−85.

(4) Matsumoto, M., and Miwa, M. (1973) Study on the new phospholipid, N-acyl-I-alkyl glycerophosphorylethanolamine, from bovine erythrocytes. *Biochim. Biophys. Acta 296*, 350−364.

(5) Epps, D. E., Natarajan, V., Schmid, P. C., and Schmid, H. O. (1980) Accumulation of N-acylethanolamine glycerophospholipids in infarcted myocardium. *Biochim. Biophys. Acta 618*, 420−430.

(6) Sandoval, J. A., Huang, Z. H., Garrett, D. C., Gage, D. A., and Chapman, K. D. (1995) N-Acylphosphatidylethanolamine in dry and imbibing cottonseeds. Amounts, molecular species, and enzymatic synthesis. *Plant Physiol. 109*, 269−275.

(7) Shangguan, T., Pak, C. C., Ali, S., Janoff, A. S., and Meers, P. (1998) Cation-dependent fusogenicity of an N-acyl phosphatidylethanolamine. *Biochim. Biophys. Acta 1368*, 171−183.

(8) Gillum, M. P., Zhang, D., Zhang, X. M., Erion, D. M., Jamison, R. A., Choi, C., Dong, J., Shanabrough, M., Duenas, H. R., Frederick, D. W., Hsiao, J. J., Horvath, T. L., Lo, C. M., Tso, P., Cline, G. W., and Shulman, G. I. (2008) N-Acylphosphatidylethanolamine, a gut-derived circulating factor induced by fat ingestion, inhibits food intake. *Cell 135*, 813−824.

(9) Shiratsuchi, A., Ichiki, M., Okamoto, Y., Ueda, N., Sugimoto, N., Takuwa, Y., and Nakanishi, Y. (2009) Inhibitory effect of N-palmitoylphosphatidylethanolamine on macrophage phagocytosis through inhibition of Rac1 and Cdc42. *J. Biochem. 145*, 43−50.

(10) Ueda, N., Tsuboi, K., and Uyama, T. (2010) Enzymological studies on the biosynthesis of N-acylethanolamines. *Biochim. Biophys. Acta 1801*, 1274−1285.

(11) Schmid, P. C., Reddy, P. V., Natarajan, V., and Schmid, H. H. (1983) Metabolism of N-acylethanolamine phospholipids by a mammalian phosphodiesterase of the phospholipase D type. *J. Biol. Chem. 258*, 9302−9306.

(12) Okamoto, Y., Morishita, J., Tsuboi, K., Tonai, T., and Ueda, N. (2004) Molecular characterization of a phospholipase D generating anandamide and its congeners. *J. Biol. Chem. 279*, 5298−5305.

(13) Leung, D., Saghatelian, A., Simon, G. M., and Cravatt, B. F. (2006) Inactivation of N-acyl phosphatidylethanolamine phospholipase D reveals multiple mechanisms for the biosynthesis of endocannabinoids. *Biochemistry 45*, 4720−4726.

(14) Tsuboi, K., Okamoto, Y., Ikematsu, N., Inoue, M., Shimizu, Y., Uyama, T., Wang, J., Deutsch, D. G., Burns, M. P., Ulloa, N. M., Tokumura, A., and Ueda, N. (2011) Enzymatic formation of N-acylethanolamines from N-acylethanolamine plasmalogen through N-acylphosphatidylethanolamine-hydrolyzing phospholipase D-dependent and -independent pathways. *Biochim. Biophys. Acta 1811*, 565−577.

(15) Natarajan, V., Schmid, P. C., Reddy, P. V., and Schmid, H. H. (1984) Catabolism of N-acylethanolamine phospholipids by dog brain preparations. *J. Neurochem. 42*, 1613−1619.

(16) Sun, Y. X., Tsuboi, K., Okamoto, Y., Tonai, T., Murakami, M., Kudo, I., and Ueda, N. (2004) Biosynthesis of anandamide and N-palmitoylethanolamine by sequential actions of phospholipase A2 and lysophospholipase D. *Biochem. J. 380*, 749−756.

(17) Simon, G. M., and Cravatt, B. F. (2006) Endocannabinoid biosynthesis proceeding through glycerophospho-N-acyl ethanolamine and a role for alpha/beta-hydrolase 4 in this pathway. *J. Biol. Chem. 281*, 26465−26472.

(18) Liu, J., Wang, L., Harvey-White, J., Osei-Hyiaman, D., Razdan, R., Gong, Q., Chan, A. C., Zhou, Z., Huang, B. X., Kim, H. Y., and Kunos, G. (2006) A biosynthetic pathway for anandamide. *Proc. Natl. Acad. Sci. U.S.A. 103*, 13345−13350.

(19) Liu, J., Wang, L., Harvey-White, J., Huang, B. X., Kim, H. Y., Luquet, S., Palmiter, R. D., Krystal, G., Rai, R., Mahadevan, A., Razdan, R. K., and Kunos, G. (2008) Multiple pathways involved in the biosynthesis of anandamide. *Neuropharmacology 54*, 1−7.

(20) Natarajan, V., Reddy, P. V., Schmid, P. C., and Schmid, H. H. (1982) N-Acylation of ethanolamine phospholipids in canine myocardium. *Biochim. Biophys. Acta 712*, 342−355.

(21) Cadas, H., Gaillet, S., Beltramo, M., Venance, L., and Piomelli, D. (1996) Biosynthesis of an endogenous cannabinoid precursor in neurons and its control by calcium and cAMP. *J. Neurosci. 16*, 3934−3942.

(22) Reddy, P. V., Natarajan, V., Schmid, P. C., and Schmid, H. H. (1983) N-Acylation of dog heart ethanolamine phospholipids by transacylase activity. *Biochim. Biophys. Acta 750*, 472−480.

(23) Cadas, H., di Tomaso, E., and Piomelli, D. (1997) Occurrence and biosynthesis of endogenous cannabinoid precursor, N-arachidonoyl phosphatidylethanolamine, in rat brain. *J. Neurosci. 17*, 1226−1242.

(24) Schmid, H. H. (2000) Pathways and mechanisms of N-acylethanolamine biosynthesis: can anandamide be generated selectively? *Chem. Phys. Lipids 108*, 71−87.

(25) Jin, X. H., Okamoto, Y., Morishita, J., Tsuboi, K., Tonai, T., and Ueda, N. (2007) Discovery and characterization of a Ca^{2+}-independent phosphatidylethanolamine N-acyltransferase generating the anandamide precursor and its congeners. *J. Biol. Chem. 282*, 3614−3623.

(26) Shinohara, N., Uyama, T., Jin, X. H., Tsuboi, K., Tonai, T., Houchi, H., and Ueda, N. (2011) Enzymological analysis of the tumor suppressor A-C1 reveals a novel group of phospholipid-metabolizing enzymes. *J. Lipid Res. 52*, 1927−1935.

(27) Jin, X. H., Uyama, T., Wang, J., Okamoto, Y., Tonai, T., and Ueda, N. (2009) cDNA cloning and characterization of human and mouse Ca^{2+}-independent phosphatidylethanolamine N-acyltransferases. *Biochim. Biophys. Acta 1791*, 32−38.

(28) Uyama, T., Morishita, J., Jin, X. H., Okamoto, Y., Tsuboi, K., and Ueda, N. (2009) The tumor suppressor gene H-Rev107 functions as a novel Ca^{2+}-independent cytosolic phospholipase A1/2 of the thiol hydrolase type. *J. Lipid Res. 50*, 685−693.

(29) Uyama, T., Jin, X. H., Tsuboi, K., Tonai, T., and Ueda, N. (2009) Characterization of the human tumor suppressors TIG3 and HRASLS2 as phospholipid-metabolizing enzymes. *Biochim. Biophys. Acta 1791*, 1114−1124.

(30) Uyama, T., Inoue, M., Okamoto, Y., Shinohara, N., Tai, T., Tsuboi, K., Inoue, T., Tokumura, A., and Ueda, N. (2013) Involvement of phospholipase A/acyltransferase-1 in N-acylphosphatidylethanolamine generation. *Biochim. Biophys. Acta 1831*, 1690−1701.

(31) Uyama, T., Ikematsu, N., Inoue, M., Shinohara, N., Jin, X. H., Tsuboi, K., Tonai, T., Tokumura, A., and Ueda, N. (2012) Generation of N-acylphosphatidylethanolamine by members of the phospholipase A/acyltransferase (PLA/AT) family. *J. Biol. Chem. 287*, 31905−31919.

(32) Golczak, M., Kiser, P. D., Sears, A. E., Lodowski, D. T., Blaner, W. S., and Palczewski, K. (2012) Structural basis for the acyltransferase activity of lecithin:retinol acyltransferase-like proteins. *J. Biol. Chem. 287*, 23790−23807.

(33) Guan, Z., Li, S., Smith, D. C., Shaw, W. A., and Raetz, C. R. (2007) Identification of N-acylphosphatidylserine molecules in eukaryotic cells. *Biochemistry 46*, 14500−14513.

(34) Wood, P. L. (2014) Accumulation of N-acylphosphatidylserines and N-acylserines in the frontal cortex in schizophrenia. *Neurotransmitter 1*, 10−14800/nt 14263..

(35) Simon, G. M., and Cravatt, B. F. (2008) Anandamide biosynthesis catalyzed by the phosphodiesterase GDE1 and detection of glycerophospho-N-acyl ethanolamine precursors in mouse brain. *J. Biol. Chem. 283*, 9341−9349.

(36) Bartlett, G. R. (1959) Phosphorus assay in column chromatography. *J. Biol. Chem. 234*, 466−468.

(37) Kamat, S. S., and Camara, K. (2015) Immunomodulatory lysophosphatidylserines are regulated by ABHD16A and ABHD12 interplay. *Nat. Chem. Biol. 11*, 164−171.

DOI: 10.1021/acs.biochem.5b00207
Biochemistry 2015, 54, 2539−2549

(38) Jessani, N., Niessen, S., Wei, B. Q., Nicolau, M., Humphrey, M., Ji, Y., Han, W., Noh, D. Y., Yates, J. R., III, Jeffrey, S. S., and Cravatt, B. F. (2005) A streamlined platform for high-content functional proteomics of primary human specimens. *Nat. Methods 2*, 691−697.
(39) Bligh, E. G., and Dyer, W. J. (1959) A rapid method of total lipid extraction and purification. *Can. J. Biochem. Physiol. 37*, 911−917.
(40) Saghatelian, A., Trauger, S. A., Want, E. J., Hawkins, E. G., Siuzdak, G., and Cravatt, B. F. (2004) Assignment of endogenous substrates to enzymes by global metabolite profiling. *Biochemistry 43*, 14332−14339.
(41) Tautenhahn, R., Patti, G. J., Rinehart, D., and Siuzdak, G. (2012) XCMS Online: a web-based platform to process untargeted metabolomic data. *Anal. Chem. 84*, 5035−5039.
(42) Smith, C. A., Want, E. J., O'Maille, G., Abagyan, R., and Siuzdak, G. (2006) XCMS: processing mass spectrometry data for metabolite profiling using nonlinear peak alignment, matching, and identification. *Anal. Chem. 78*, 779−787.
(43) Simon, G. M., and Cravatt, B. F. (2010) Characterization of mice lacking candidate N-acyl ethanolamine biosynthetic enzymes provides evidence for multiple pathways that contribute to endocannabinoid production in vivo. *Mol. BioSyst. 6*, 1411−1418.
(44) Dawson, R. M. (1960) A hydrolytic procedure for the identification and estimation of individual phospholipids in biological samples. *Biochem. J. 75*, 45−53.
(45) Folch, J., Lees, M., and Sloane Stanley, G. H. (1957) A simple method for the isolation and purification of total lipides from animal tissues. *J. Biol. Chem. 226*, 497−509.
(46) Milman, G., Maor, Y., Abu-Lafi, S., Horowitz, M., Gallily, R., Batkai, S., Mo, F. M., Offertaler, L., Pacher, P., Kunos, G., and Mechoulam, R. (2006) N-Arachidonoyl L-serine, an endocannabinoid-like brain constituent with vasodilatory properties. *Proc. Natl. Acad. Sci. U.S.A. 103*, 2428−2433.
(47) Cohen-Yeshurun, A., Willner, D., Trembovler, V., Alexandrovich, A., Mechoulam, R., Shohami, E., and Leker, R. R. (2013) N-arachidonoyl-L-serine (AraS) possesses proneurogenic properties in vitro and in vivo after traumatic brain injury. *J. Cereb. Blood Flow Metab. 33*, 1242−1250.
(48) Cohen-Yeshurun, A., Trembovler, V., Alexandrovich, A., Ryberg, E., Greasley, P. J., Mechoulam, R., Shohami, E., and Leker, R. R. (2011) N-Arachidonoyl-L-serine is neuroprotective after traumatic brain injury by reducing apoptosis. *J. Cereb. Blood Flow Metab. 31*, 1768−1777.
(49) Smoum, R., Bar, A., Tan, B., Milman, G., Attar-Namdar, M., Ofek, O., Stuart, J. M., Bajayo, A., Tam, J., Kram, V., O'Dell, D., Walker, M. J., Bradshaw, H. B., Bab, I., and Mechoulam, R. (2010) Oleoyl serine, an endogenous N-acyl amide, modulates bone remodeling and mass. *Proc. Natl. Acad. Sci. U.S.A. 107*, 17710−17715.
(50) Guan, Z. (2009) Discovering novel brain lipids by liquid chromatography/tandem mass spectrometry. *J. Chromatogr. B: Anal. Technol. Biomed. Life Sci. 877*, 2814−2821.
(51) Simpson, C. D., Hurren, R., Kasimer, D., MacLean, N., Eberhard, Y., Ketela, T., Moffat, J., and Schimmer, A. D. (2012) A genome wide shRNA screen identifies alpha/beta hydrolase domain containing 4 (ABHD4) as a novel regulator of anoikis resistance. *Apoptosis 17*, 666−678.

DOI: 10.1021/acs.biochem.5b00207
Biochemistry 2015, 54, 2539−2549